PHYSICAL REVIEW B **81**, 104416 (2010)

Electronic structure and magnetic properties of the spin-gap compound $Cu_2(PO_3)_2CH_2$: Magnetic versus structural dimers

M. Schmitt,[1] A. A. Gippius,[1,2] K. S. Okhotnikov,[2] W. Schnelle,[1] K. Koch,[1] O. Janson,[1] W. Liu,[1] Y.-H. Huang,[1] Y. Skourski,[3] F. Weickert,[1,3] M. Baenitz,[1] and H. Rosner[1]

[1]*Max Planck Institute for Chemical Physics of Solids, 01187 Dresden, Germany*

[2]*Moscow State University, 119992 Moscow, Russia*

[3]*Dresden High Magnetic Field Laboratory, 01328 Dresden, Germany*

(Received 7 December 2009; revised manuscript received 29 January 2010; published 18 March 2010)

A joint experimental and theoretical investigation of the spin 1/2 system $Cu_2(PO_3)_2CH_2$ suggests a description of this compound as coupled alternating antiferromagnetic Heisenberg chains. Magnetic susceptibility, specific heat, nuclear magnetic resonance, nuclear quadrupole resonance, and high-field magnetization measurements evidence a spin gap of about 25 K. Surprisingly, the leading antiferromagnetic exchange of about 75 K can be assigned by density-functional band-structure calculations to a coupling between the structural Cu_2O_6 dimers, whereas the coupling within these dimers is strongly reduced due to sizable ferromagnetic contributions. The coupling within the structural dimers competes with a number of long-range couplings. The present available experimental data can be consistently described in a scenario of coupled alternating chains. The proposed model should be considered as a minimal model for an appropriate description of this compound.

DOI: 10.1103/PhysRevB.81.104416 PACS number(s): 75.47.Pq, 75.30.Et

I. INTRODUCTION

Due to their large variety of unprecedented exotic ground states, low-dimensional magnetic compounds have always attracted great interest in solid-state physics and chemistry. For low dimensions and spin 1/2, the influence of quantum fluctuations becomes crucial for the ground state of the system. The role of quantum fluctuations is even more pronounced if the system under consideration exhibits strongly frustrated interactions. In general, the frustration can raise from purely geometrically frustrated lattices such as triangular and Kagomé lattices or from competing inequivalent interactions like in quasi-one-dimensional (quasi-1D) chains with sizable antiferromagnetic (AFM) second-neighbor interactions. It is obvious that the crystal structure of a compound is the key for the understanding of its magnetic properties. On the other hand, it is far from trivial to derive the appropriate magnetic model just from structural considerations. The results of such an analysis may be completely misleading as was the case for the system $(VO)_2P_2O_7$.[1,2]

Even careful interpretations based on accurate experimental data, but within a limited spectrum of methods, have suggested controversially debated magnetic models for several compounds in the recent years.[3–12] The difficulty to establish the correct magnetic model and to estimate its relevant exchange parameters unambiguously is often connected to internal symmetries of the model itself. Due to such symmetries, experimental data can be fitted with different sets of parameters belonging to essentially different regions in the phase diagram. Prominent representatives for this problem are, for instance, the J_1-J_2 chain compound $LiCu_2O_2$ (Refs. 6–9) or the frustrated square-lattice system Li_2VOSiO_4.[3–5] These controversies underline the importance of applying different independent methods to establish the correct magnetic model for a new material. In particular, the search for the proper magnetic model can largely benefit from the combination of various experimental methods with a detailed microscopic analysis based on modern band-structure theory.[10–12]

In the present paper, we demonstrate that such a combination of independent methods leads to a consistent physical picture even for a material with a rather complex crystal structure including (i) local distortion around the magnetic sites, (ii) competing ferromagnetic (FM) and antiferromagnetic interactions due to the vicinity of the Cu-O-Cu bond angle to 90°, and (iii) numerous inequivalent superexchange pathways. We apply nuclear magnetic resonance (NMR) and nuclear quadrupole resonance (NQR) spectroscopy, magnetic susceptibility, specific-heat, and high-field magnetization measurements together with extensive electronic structure calculations for the recently studied spin 1/2 compound $Cu_2(PO_3)_2CH_2$ (Ref. 13) to answer the question whether the structural dimers in this material should be considered as magnetic dimers and lead to a spin model of weakly coupled dimers.

The crystal structure of $Cu_2(PO_3)_2CH_2$ contains pairs of strongly distorted edge-sharing CuO_4 plaquettes connected with each other by $PO_3CH_2PO_3$ units (Fig. 1). These structural Cu_2O_6 dimers with Cu-O-Cu bond angles of 101° and 94° form chains along the crystallographic *b* direction. Regarding the dimers and their arrangement, the crystal structure of $Cu_2(PO_3)_2CH_2$ strongly resembles the compounds $Na_3Cu_2SbO_6$ and $Na_2Cu_2TeO_6$ which have been discussed recently as quasi-1D alternating chain materials.[14–16] However, up to now no consensus is obtained with respect to the nature of the alternating couplings in these compounds. This emphasizes the above-mentioned importance of a versatile approach.

The presented joint experimental and theoretical study of $Cu_2(PO_3)_2CH_2$ yields a picture of coupled alternating chains. These alternating chains are formed by weakly coupled magnetic dimers, which surprisingly do not coincide with the structural dimers as one may expect in a naive approach.

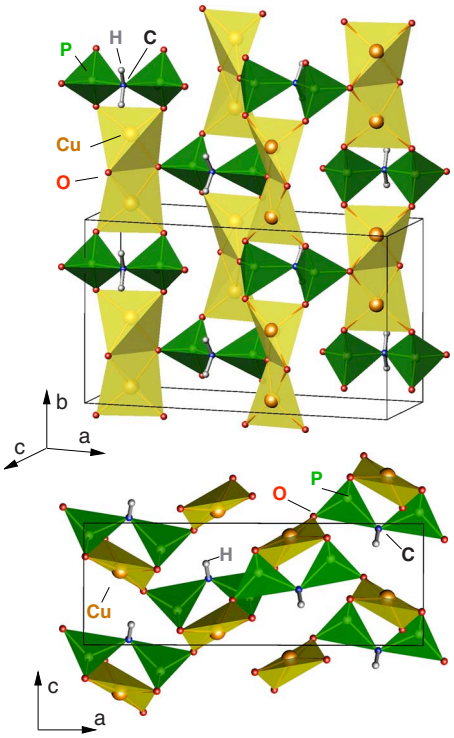

FIG. 1. (Color online) Crystal structure of $Cu_2(PO_3)_2CH_2$. Cu atoms (large orange spheres) are coordinated tetrahedrally by O atoms (small red spheres on tetrahedron corners) and form structural dimers. These Cu_2O_6 dimers are connected via $PO_3CH_2PO_3$ units with two crystallographically inequivalent P positions.

Such a difference between structural and magnetic dimers was already observed in $VO(HPO_4)\cdot H_2O$.[17]

II. METHODS

A. Experiments

$Cu_2(PO_3)_2CH_2$ has been prepared under mild hydrothermal conditions at 433 K from a mixture of $Cu(CH_3COO)_2\cdot H_2O$ (2.0 g, 10 mmol), H_3BO_3 (0.62 g, 10 mmol), and methylenediphonic acid (1.76 g, 10 mmol) with a molar ratio of 1:1:1. At first, the mixture was dissolved in 10 ml H_2O and stirred at 333 K for 2 h; then the resulting clear green solution was transferred into a 25 ml Teflon autoclave (degree of filling: 70%) and held at 433 K for 5 days under autogenous pressure. Finally, crystals of $Cu_2(PO_3)_2CH_2$ were filtered, washed with deionized water and dried at 333 K in air.

The crystal structure was determined by x-ray diffraction to be within the orthorhombic *Pnma* group with the lattice parameters $a=13.696(2)$ Å, $b=8.0103(13)$ Å, and $c=4.9034(7)$ Å. The refined lattice parameters and Wykhoff positions are in reasonable agreement with earlier studies.[13,18]

The magnetization of the compound (small light-brown colored crystals) was measured in a superconducting quantum interference device (SQUID) magnetometer (MPMS XL-7, Quantum Design) in magnetic fields $\mu_0 H$ between 0.01 and 7 T ($T=1.8-400$ K).

High-field magnetization measurements were carried out at the Dresden High Magnetic Field Laboratory (HLD) in pulsed fields up to 60 T with a typical pulse duration of 50 ms. A high precision pick-up coil device[19] was used, mounted in a ^{4}He-flow cryostat. A powdered sample of several milligrams was measured at the lowest available temperature of 1.5 K.

The heat capacity was determined by a relaxation-type method (PPMS, Quantum Design) in magnetic fields up to $\mu_0 H=9$ T ($T=1.8-320$ K) on four larger crystal aggregates ($m=6.632$ mg). The NMR measurements were performed with a conventional pulsed NMR spectrometer (Tecmag Apollo) in the temperature range 1.8–200 K. ^{31}P NMR spectra were obtained by Fourier transformation of a half of the spin echo in external magnetic field of 4.093 T. ^{63,65}Cu NQR spectra were measured both by Fourier transform and point-by-point frequency step methods. ^{63}Cu spin-lattice-relaxation data were obtained by the saturation recovery method.

B. Calculations

For the electronic band-structure calculations a full-potential nonorthogonal local-orbital (FPLO) minimum-basis scheme within the local-density approximation was used.[20] To treat the short C-H distance (0.96 Å) the version FPLO6.00-24, with its double numerical basis for the valence states was used. In the scalar relativistic calculation the exchange and correlation functional of Perdew and Wang has been applied.[21]

To study the magnetic properties of the system we mapped the local (spin) density approximation [L(S)DA] band structure onto an effective one-band tight-binding (TB) model based on Cu-site centered Wannier functions. Strong correlations were included by mapping the TB model onto a Hubbard model and subsequently onto a Heisenberg model. In addition, LSDA+U (Ref. 22) calculations of supercells with various collinear spin arrangements have been carried out. To approximate the strong Coulomb repulsion at the Cu 3d orbitals in a mean field way a Coulomb parameter $U_d=6.0-7.5$ eV and an onsite exchange $J=1$ eV were used within the around-mean-field double-counting scheme.[23]

To calculate the electric field gradient (EFG), we used the recently implemented EFG module for the FPLO code[24,25] within the LDA and LSDA+U approximations in a wide range of U_d ($U_d=3.5-7.5$ eV).

Quantum Monte Carlo (QMC) simulations were performed on a cluster of $N=480$ spins $S=1/2$ (12 coupled chains of 40 sites each) using the ALPS code.[26] To diminish statistical errors, we used 150 000 sweeps for thermalization and 1 500 000 sweeps after thermalization in the temperature range $T/J=0.03-5$.

III. RESULTS AND DISCUSSION

A. Magnetic susceptibility and specific heat

The magnetic susceptibility (Fig. 2) shows a broad maximum at 45 K and a Curie-Weiss-type decrease at high temperatures. This behavior is not changed by the variation of the external field. A Curie-Weiss fit (range 120–400 K; full

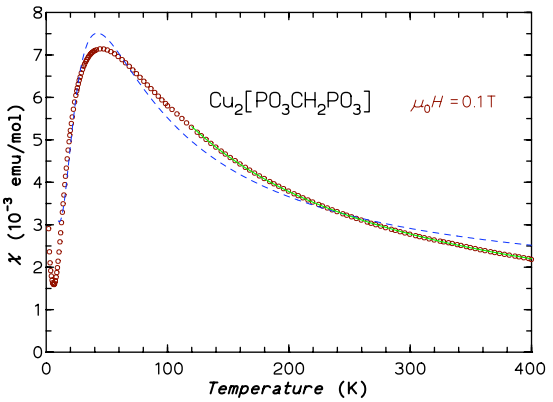

FIG. 2. (Color online) Magnetic susceptibility of $Cu_2(PO_3)_2CH_2$ for $\mu_0 H=0.1$ T. The full line shows the Curie-Weiss fit in the range 120–400 K, the dashed line the magnetic dimer model fit.

line in Fig. 2) results in $\mu_{\text{eff}}=2.90\mu_B$/f.u. (corresponding to $\mu_{\text{eff}}=2.05\mu_B$/Cu) and a large Weiss temperature $\theta_{\text{CW}}=-78$ K. At low temperatures $\chi(T)$ decreases strongly which suggests the presence of a spin gap. At the lowest temperature a Curie-type upturn becomes visible which is probably due to impurities and point defects. No magnetic ordering is observed above 1.8 K, in contrast to the interpretation of the magnetization data by Barthelet *et al.*[13]

Due to the edge sharing of two neighboring CuO_4 coordination tetrahedra, these Cu_2O_6 units can be described as structural dimers. Therefore, one may assume that these magnetic species also behave as magnetic dimers with dominant Cu-O-Cu exchange paths via the two O species. A fit of $\chi(T)$ with the Bleaney-Bowers model,[27] including a Curie term C/T for the defects and a constant χ_0, was attempted (dashed line in Fig. 2). It results in a very low g-factor and $J\approx-35$ K, but it definitively does not describe the data. Thus, a less obvious magnetic exchange model is realized in $Cu_2(PO_3)_2CH_2$. Further fits of the data are shown in Sec. III D (see Fig. 13).

The molar specific heat is given in Fig. 3. There is no visible anomaly as an indication of a long-range magnetic order, but $c_p(T)$ is dominated by a broad Schottky-type anomaly with maximum at about 20 K in c_p/T, which is

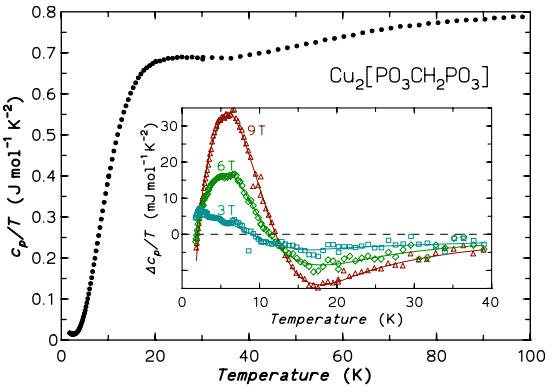

FIG. 3. (Color online) Specific heat c_p/T of $Cu_2(PO_3)_2CH_2$ in zero magnetic field. Inset: differences $\Delta c_p(H)/T$ of the specific heat in magnetic fields to the zero-field data.

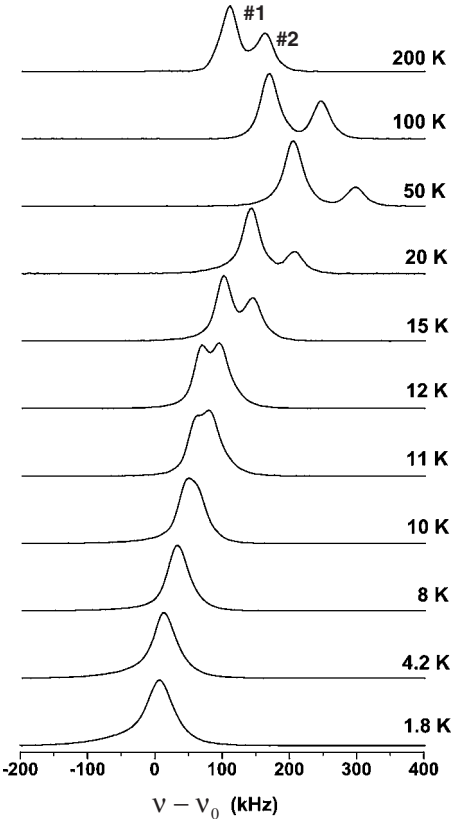

FIG. 4. Temperature dependence of the ^{31}P NMR spectra at $\mu_0 H=4.093$ T. The two signals of the in-equivalent P sites are denoted with #1 and #2. The reference frequency ν_0 is 70.0 MHz and the ^{31}P Larmor frequency $\nu_L=70.543$ MHz.

probably due to thermal excitation over the spin gap. The determination of the lattice and magnetic contribution to $c_p(T)$ of this compound is problematic without a proper lattice reference compound. The field dependence of c_p/T (inset of Fig. 3) is quite small. The entropy, shifted due to the application of our maximum magnetic field (9 T), yields less than 2% of the total magnetic entropy of $2R$ ln 2.

B. ^{31}P NMR Knight shift

Above $T_c\approx10$ K the ^{31}P NMR spectra consist of two distinct peaks, which are due to two nonequivalent crystallographic P sites (Fig. 4 and compare Fig. 1). At low temperatures these peaks can be approximated by Gaussian lines with almost equal integral intensity, reflecting equal occupation factors of the P sites. At high temperatures the integral intensities of the two ^{31}P NMR signals are different which could be ascribed to a T_2 effect: due to the complicated Cu-O-Cu and Cu-O-P-O-Cu superexchange interaction paths (see below), the ^{31}P spin-spin relaxation time T_2 at the two P sites is not equivalent. Dissimilar T_2 values result in different spin-echo intensities for the two P sites at fixed pulse separation time. Since the ^{31}P spin-lattice relaxation rate $^{31}(1/T_1)$ decreases exponentially with temperature, this effect vanishes at low temperatures. Below about 10 K both peaks become indistinguishable (Figs. 4 and 5). Since the two peaks of the ^{31}P NMR spectrum have essentially the same

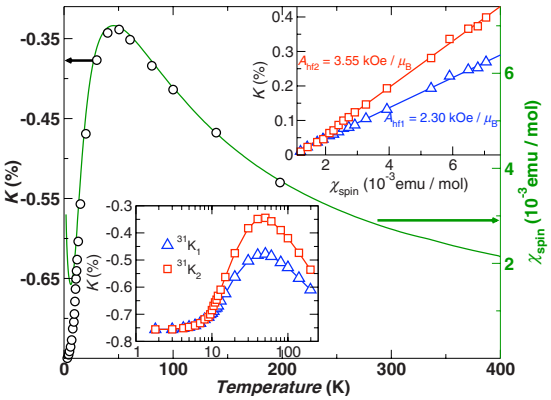

FIG. 5. (Color online) Temperature dependence of the magnetic susceptibility χ (solid line) and the Knight shift K of the right ^{31}P NMR signal (circles) denoted as $^{31}K_2$. Upper inset: K_{spin} vs χ plot for both ^{31}P lines. Lower inset: comparison of the Knight shift for both ^{31}P lines as a function of temperature.

temperature dependence of the line shift, the right (high-frequency) peak was used for the data evaluation. The temperature dependence of the Knight shift, $K(T)$, is typical for low-dimensional systems, exhibiting a broad maxima at 40–50 K and a rapid decrease at low temperatures (Fig. 5). Such behavior is a clear evidence for a singlet ground state with a gap in the magnetic excitation spectrum.

The line shift K as a function of temperature for the right signal is shown in Fig. 5. In general, the total observed shift K can be decomposed into a temperature-independent orbital contribution K_{orb} and a spin term K_{spin}. Therefore, for each ^{31}P NMR line one can write

$$K_1(T) = K_{1orb} + A_{hf1} \cdot \chi_{spin}(T), \tag{1}$$

$$K_2(T) = K_{2orb} + A_{hf2} \cdot \chi_{spin}(T), \tag{2}$$

where A_{hf1} and A_{hf2} are the hyperfine coupling constants. Since the temperature-dependent component of the line shift is proportional to the spin part of the magnetic susceptibility, it enables us to avoid the impurity upturn observed at low temperatures in the bulk magnetic susceptibility measurements [see Fig. 2 (circles) and Fig. 5 (solid line)]. The orbital contribution to the total shift is equal for both lines $K_{1orb} = K_{2orb} = K_{orb}$. Thus, only the second term in Eq. (2) depends on the spin susceptibility. The values of $A_{hf1} = 0.230$ T/μ_B and $A_{hf2} = 0.355$ T/μ_B were determined from the K vs χ plot (see the upper inset in Fig. 5). For this procedure the low-temperature impurity Curie-type upturn was subtracted from the $\chi(T)$ data. The resulting higher hyperfine value A_{hf2} of the right (high-frequency) ^{31}P NMR signal is consistent with the shorter T_2 value of this line and causes its smaller integral intensity at high temperatures.

A fit of the $K(T)$ dependence within a simple dimer model showed large systematic deviations from the experimental data, as already seen for the bulk susceptibility data (Fig. 2). Therefore, a magnetic dimer model assuming essentially isolated structural Cu dimers can be ruled out.

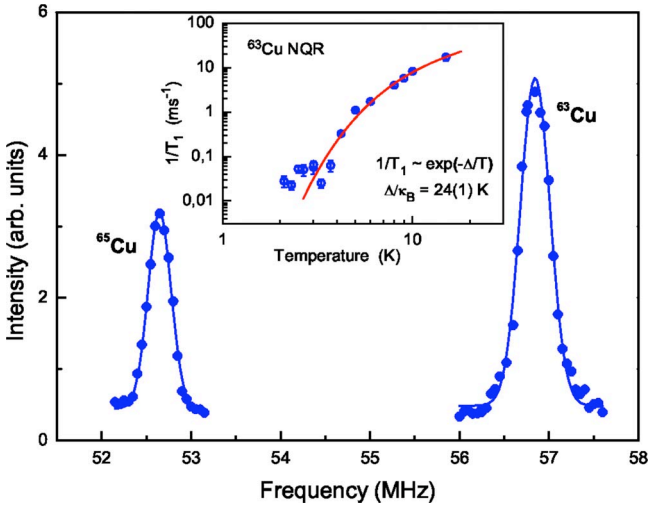

FIG. 6. (Color online) NQR spectrum of ^{63,65}Cu in $Cu_2(PO_3)_2CH_2$. The solid lines are the Gaussian fits. Inset: temperature dependence of the ^{63}Cu nuclear spin-lattice-relaxation rate. The solid line is the best fit to the activation law.

C. ^{63,65}Cu NQR

The NQR spectrum of ^{63,65}Cu in $Cu_2(PO_3)_2CH_2$ at 4.2 K is shown in Fig. 6. The ratio of the resonance frequencies (56.85 and 52.60 MHz) and the intensities of the lines correlate well with the ratio of the quadrupole moments and the natural abundance for ^{63}Cu and ^{65}Cu isotopes, respectively. The striking features of the observed NQR spectrum are the very high values of the ^{63,65}Cu quadrupole frequency in $Cu_2(PO_3)_2CH_2$ in comparison to NQR frequencies of known cuprates.[28,29]

The quadrupole frequency is composed of two terms

$$\nu_Q = \nu_{on\text{-}site} + \nu_{ion}(1 - \gamma_\infty), \tag{3}$$

where $\nu_{on\text{-}site}$ is the valence contribution caused by the incomplete filling of the $3d$ electronic shell of Cu, ν_{ion} is the contribution from the surrounding ions assuming their formal valencies, and $(1-\gamma_\infty)$ is the Sternheimer factor taking into account the polarization of the inner Cu shells by the ionic EFG. It is known that one hole in the $3d_{x^2-y^2}$ orbital ($3d^9$), the electronic configuration of the magnetic Cu^{2+} ion, gives $\nu_{on\text{-}site}(3d^9) = -117.1$ MHz.[30] Considering the strong distortion of the CuO_4 plaquettes we expect a sizable admixture of all $3d$ orbitals to the magnetically active state, resulting in their strong on-site contribution to the NQR frequency.

The nuclear spin-lattice relaxation (SLR) provides one of the most crucial tests for any theoretical model of spin fluctuations since it probes the fluctuations of the hyperfine field at the nuclear site. The nuclear SLR measurements were performed on the ^{63}Cu isotope.

The temperature dependence of the ^{63}Cu SLR rate $^{63}(1/T_1)$ was obtained in the temperature range 2–20 K (see inset in Fig. 6). The SLR seems to be the sum of two processes: (i) an activation process, which freezes out at low temperatures and (ii) temperature-independent quantum spin fluctuations. Above 4 K the $^{63}(1/T_1)$ exhibits an activation

law $\exp(-\Delta/T)$ with the gap value of $\Delta_{^{63}(1/T_1)}=24(1)$ K. Below 4 K the ^{63}Cu SLR rate becomes almost temperature independent with a value of about 30 s^{-1}.

The almost constant and relatively high values of ^{63}Cu SLR rate are observed below 4 K where the thermal spin excitations across the gap are essentially frozen and therefore the activated spin-lattice-relaxation mechanism is vanishing. This is seen in the inset in Fig. 6, where the solid curve corresponding to the (thermal) activation law drops below the experimental $1/T_1$ data points at temperatures $T<3$ K. Therefore, only quantum spin fluctuations contribute essentially to $1/T_1$ at low temperatures.[31]

A finite SLR behavior at low temperatures was theoretically estimated and experimentally observed by Ehrenfreund *et al.*[32] for organic spin-1/2 Heisenberg 1D antiferromagnets. Later, Sachdev[33] determined the temperature dependence of the nuclear SLR $1/T_1$ for half-integer spin chains for $k_BT/J \ll 1$ as $1/T_1=$const. Quantum Monte Carlo calculations by Sandvik[34] support these results for the low-temperature limit. The SLR rate, in general, is affected by both uniform (at wave vector $q=0$) and on-site staggered spin fluctuations at $q=\pm\pi/a$. The uniform component leads to $1/T_1 \sim T$ and is negligible at $T \to 0$, while the staggered component gives $1/T_1=$const. and dominates at low temperatures.[33] Almost temperature-independent Cu nuclear SLR was observed experimentally by Ishida *et al.*[35] in the linear spin-chain compound Ca_2CuO_3. Recently, a comparable SLR on Cu was experimentally observed for the inorganic compound $CuSiO_3$, isostructural to the Spin-Peierls system $CuGeO_3$,[36] as well for ^{31}P SLR in $Sr_2Cu(PO_4)_2$ and $Ba_2Cu(PO_4)_2$.[37]

For $Cu_2(PO_3)_2CH_2$ a similar SLR behavior is found, but could be caused, as suggested by the band-structure calculations (see next section), by a more three-dimensional exchange scenario in connection with sizable magnetic frustration as the origin of nonfreezing quantum spin fluctuations. The latter scenario is supported by a slight deviation of the low-temperature $1/T_1$ data from a constant value toward a power-law $1/T_1 \sim T^n$ with $0<n<1$ (see inset in Fig. 6).

D. Microscopic modeling

1. Band-structure calculations—LDA

To get microscopic insight into the electronic structure, the relevant orbitals and main interaction paths, density-functional band-structure calculations were carried out. In Fig. 7 the total and atom-resolved density of states (DOS) are shown. The valence band of $Cu_2(PO_3)_2CH_2$ has a width of about 10 eV and splits in clearly separated parts, which can be assigned to the states of the different structural building blocks. Between −5 and 1 eV the states are dominated by the CuO-plaquette states. The lower lying states between −5 and −7.5 eV and between −8 and −10 eV originate mainly from PO_3 and CH_2 contributions. The contributions of P, C, and H states in the energy range from −1 to 0.4 eV are negligible.

Typical for undoped cuprates, we find metallic behavior as the antibonding Cu-O related bands cross the Fermi level. The metallic behavior is in contradiction with the insulating behavior concluded from the transparent light-brown color of

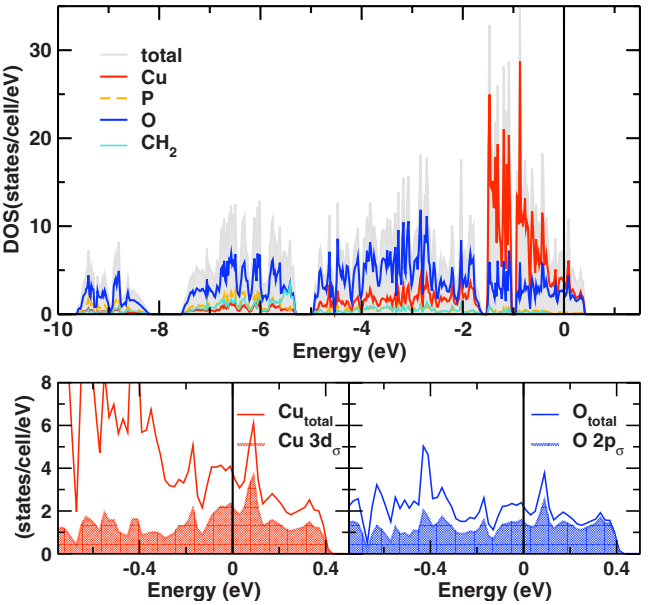

FIG. 7. (Color online) Calculated density of states (LDA) for $Cu_2(PO_3)_2CH_2$: Top: the valence band is dominated by Cu and O states. The contributions from P, C, and H in the energy range from −1 to 0.4 eV are negligible. Bottom: orbital-resolved density of states. The distortion of Cu-O plaquettes leads to a hybridization with Cu-O states, beyond the $dp\sigma$ orbital.

the sample. This discrepancy is a typical shortcoming of the LDA calculations due to the well-known underestimation of the strong Cu $3d$ correlation. Adding the missing correlations in a mean-fieldlike approach using the LSDA+U scheme or mapping the LDA bands onto an effective tight-binding model and subsequently onto a Hubbard and a Heisenberg model restores the insulating properties.

Most important for our study are the antibonding Cu-O $dp\sigma$ states as they are responsible for the magnetic properties of the system. In many cuprate systems with planar or quasiplanar Cu-O coordination[38,39] these states are well separated from the lower lying states of the valence band. In these cases, the derivation of the relevant effective TB model is rather simple. However, in $Cu_2(PO_3)_2CH_2$ the situation is more complex: the separated band complex above −1 eV (see Figs. 7 and 8) contains 24 bands instead of the expected 8 antibonding bands according to 8 Cu atoms per unit cell. Although the Cu-O $dp\sigma$ states dominate the higher lying bands (between −0.4 and 0.4 eV, see upper panel of Fig. 8), they show a sizable mixing with the nonbonding bands at lower energies. This can also be seen from the orbital-resolved DOS (see Fig. 7) where the Cu and O $dp\sigma$ states spread out to lower energies and, at the same time, the highest antibonding bands show a corresponding admixture of other Cu and O orbitals. The underlying reason for the unusually strong admixture of nonplanar orbitals is the rather strong distortion of the CuO_4 plaquettes which even renders the assignment of the Cu-O $dp\sigma$ states a bit ambiguous.

To remove the ambiguity in the selection of the relevant bands applying a least-squares TB fit procedure, we calculate the TB model parameters from the calculated Wannier func-

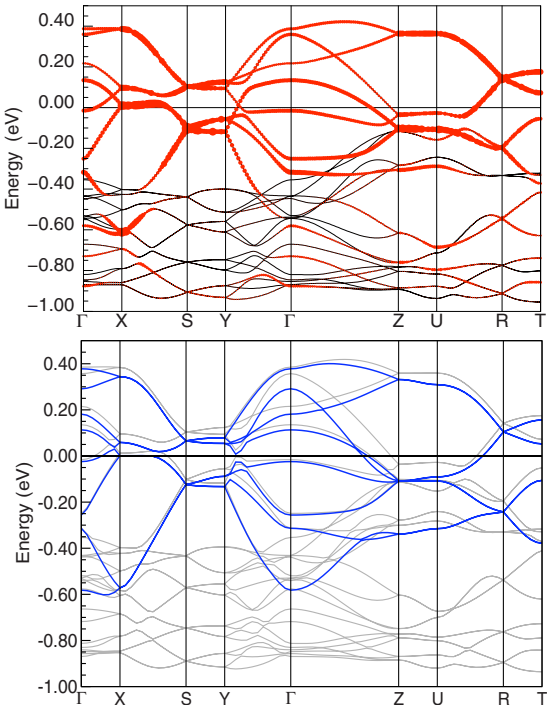

FIG. 8. (Color online) Top: calculated band structure and characters of Cu-O $dp\sigma$ states. Strong hybridization at the lower end of the $dp\sigma$ band complex caused by the distortion of plaquettes. Bottom: calculated band structure in comparison with the bands derived from Wannier functions.

tions (see Fig. 9). In Fig. 8 (lower panel), the resulting TB bands (blue) are presented together with the LDA band structure (gray). In line with the above-mentioned hybridization, the higher lying TB bands agree quite well with the underlying LDA bands, whereas a sizable deviation is observed at lower energies. With a resulting bandwidth of about 1 eV for the effective one-band model, $Cu_2(PO_3)_2CH_2$ shows a rather typical value compared to related compounds with isolated CuO_4 plaquettes as $Sr_2Cu(PO_4)_2$ [bandwidth $w \sim 0.7$ eV (Ref. 38)], Bi_2CuO_4 [$w \sim 1$ eV (Ref. 39)] or the dimer-chain compound $Na_3Cu_2SbO_6$ [$w \sim 0.7$ eV (Refs. 15 and 40)]. On

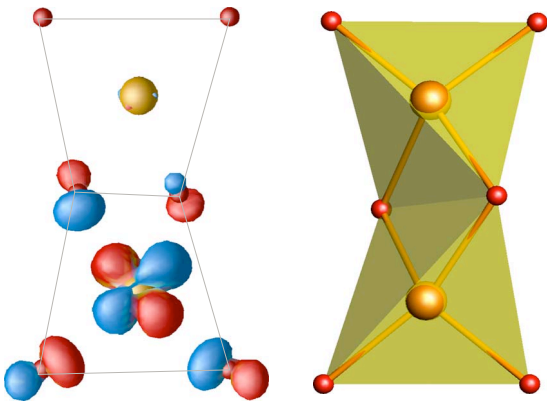

FIG. 9. (Color online) Wannier function of Cu $3d_{x^2-y^2}$ state (left) and the structural Cu_2O_6 dimer (right). The distortion of the Cu_2O_6 units leads to a deviation of the Wannier functions from a planar geometry typical for many cuprates.

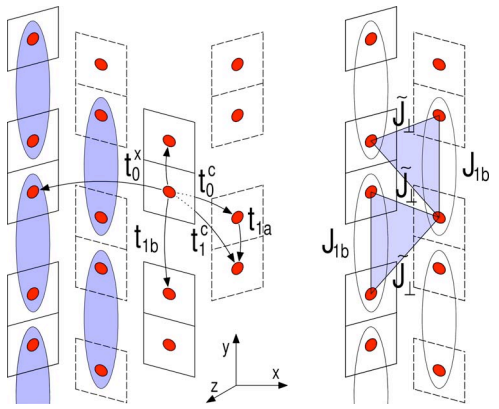

FIG. 10. (Color online) Idealized picture of the structure without distortion of the plaquettes, $PO_3CH_2PO_3$ groups are not shown. Left panel: main transfer integrals between Cu-O plaquettes from the TB model. On the left side the magnetic dimers (light blue ellipses) together with the structural dimers are depicted. Right panel: the effective frustrating interchain coupling between the dimer chains is illustrated by triangles.

the other hand, one should keep in mind that, despite the rather good matching of the TB model to the LDA bands, the accuracy of an effective one-band model is limited due to the sizable hybridization with other Cu-O orbitals not included in this model. Although, in principle, the agreement of the TB bands with the LDA calculation could be improved by an extension to a multiband model, we restrict our investigation to an effective one-band approach for the sake of simplicity and easy interpretation.

The resulting leading hopping integrals t_i from the Wannier-function-based TB model are pictured in Fig. 10. We find a clear regime of interactions where the leading transfer terms are the nearest-neighbor (NN) intradimer hopping $t_{1a}=103$ meV and the NN interdimer hopping $t_{1b}=92$ meV along the dimer chain direction. In addition, smaller interdimer couplings of the order of 50 meV perpendicular to the dimer chain with partial frustrating character are obtained. Due to the low symmetry of the distorted plaquette network (different orientation of the plaquettes), several only slightly different hopping terms are obtained. For simplification, they can be represented by the effective (averaged) parameters $\tilde{t}_i$ in good approximation (see Fig. 10).

Considering only the low-lying spin excitations, the obtained transfer integrals can be further mapped via a Hubbard to a Heisenberg model

$$\mathcal{H} = \sum_{\langle ij \rangle} J_{ij} \vec{S}_i \vec{S}_j \tag{4}$$

were the exchange integrals are obtained according to $J_{ij}=4t_{ij}^2/U_{\text{eff}}$ in the limit of strong correlations $U_{\text{eff}} \gg t_{ij}$ at half filling which is well fulfilled for $Cu_2(PO_3)_2CH_2$.

Applying $U_{\text{eff}}=4.5$ eV (Ref. 41) we obtain $J_{1a}^{\text{AFM}}=9.5$ meV and $J_{1b}^{\text{AFM}}=7.5$ meV for the leading couplings along the chains. To simplify the picture further, for the smaller, frustrating interchain couplings an averaged coupling $\tilde{J}_\perp^{\text{AFM}} \sim 1$ meV can be introduced (see Fig. 10) since

the couplings $\tilde{J}_i^{\mathrm{AFM}}$ are of rather similar size. Thus, the LDA-based TB model results in a picture of coupled, alternating AFM chains with an alternation parameter $\alpha = J_{1a}/J_{1b}$ of the order of 1.

Although the TB model provides considerable microscopic insight into the coupling regime, one should be aware that its further mapping onto a Heisenberg model yields only the AFM part of the exchange integrals. This is especially important for Cu-O-Cu bonds close to 90° that are present in our compound inside the structural dimers. According to the Goodenough-Kanamori-Anderson rules,[42] a sizable FM contribution J_{1a}^{FM} to the total intradimer exchange J_{1a} (see Fig. 10) can be expected.

2. *Band-structure calculations*—LSDA+*U*

Based on the knowledge of the short-range character of the leading interactions in $Cu_2(PO_3)_2CH_2$, we carried out LSDA+*U* calculations for supercells with different spin arrangements. Mapping the total energies of these supercells onto a Heisenberg model we can estimate total exchange integrals including both ferromagnetic and antiferromagnetic contributions. Different magnetic solutions have been obtained from self-consistent calculations choosing different initial spin configurations. As result, we find $J_{1a} \sim 0.5$ meV and $J_{1b} \sim 6$ meV for $U_d = 7.5$ eV. This underlines the relevance of FM contributions to the intradimer exchange ($J_{1a}^{\mathrm{FM}} \sim -9$ meV), whereas for the interdimer exchanges J_{1b} and $\tilde{J}_\perp$ FM contributions are of minor importance ($J_{1b}^{\mathrm{FM}} \sim -1.5$ meV). From the LDA+*U* calculations we estimate an average (effective) coupling $\tilde{J}_\perp = 1$ meV between the dimer chains[43] in agreement with $\tilde{J}_\perp^{\mathrm{AFM}} \sim 1$ meV from the TB-based results.

From these results a rather surprising picture arises: the compound can be understood as a system of interacting AFM dimers, but the magnetic and structural dimers do *not* coincide (compare Figs. 1 and 10). In addition, the weaker interdimer coupling between the chains will be frustrated (see Fig. 10, triangles in the right panel). The change in the appropriate magnetic model using a TB-based approach (only) and combining it with LSDA+*U* results emphasizes the importance of the combined approach, since otherwise contradicting results can be obtained for this type of systems.[15,16,40]

Besides in the LDA and LSDA+*U* results, the effect of the orbital mixing is also reflected in a large experimentally measured EFG.

3. *Calculation of the EFG*

As reported in Sec. III C, in comparison to NQR frequencies of other known cuprates, the quadrupole frequency of ^{63,65}Cu in $Cu_2(PO_3)_2CH_2$ is very large. Since the quadrupole frequency is determined by a product of the nuclear quadrupole moment Q and the electric field gradient V_{zz}, it is the latter that is responsible for the large frequency in this compound. To study the EFG, we performed EFG calculations on $Cu_2(PO_3)_2CH_2$ with the observed strongly distorted, edge-shared CuO_4 plaquettes and artificially flattened edge-shared CuO_4 plaquettes. As it was reported earlier in this section,

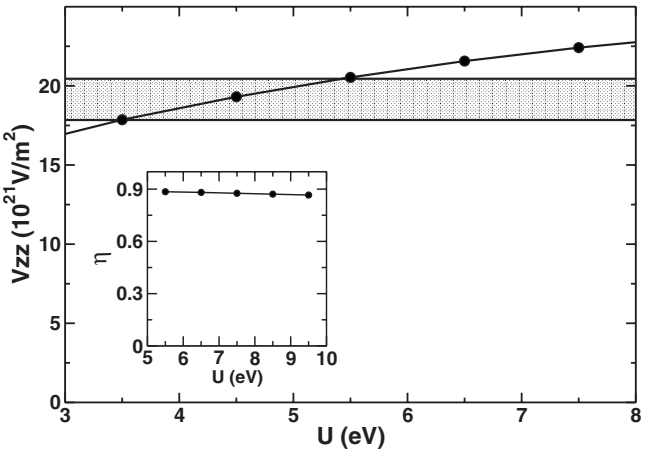

FIG. 11. Calculated EFG as a function of the Coulomb repulsion U. The experimental value for V_{zz} (using the quadrupole moment $Q = 0.220 \pm 0.015$ barn) is indicated by the shaded bar. The inset shows the weak U dependence of the asymmetry parameter η.

LDA calculations underestimate the strong Cu 3*d* correlation. This does not only affect the metallic-insulating behavior but also the EFG: as LDA results in a too small polarization of the different Cu 3*d* orbitals, the EFG for such strongly correlated systems within LDA yields values that are, in general, underestimated.[25] This is also observed here, $|V_{zz}^{\mathrm{LDA}}| = 10.3 \times 10^{21}$ V/m^2 is about a factor of two, too small compared to the experimental EFG of $|V_{zz}^{\mathrm{exp}}| = (19.0 \pm 1.3) \times 10^{21}$ V/m^2. The experimental value was calculated from the experimental frequency for ^{63}Cu (with $I = 3/2$) reported in Sec. III C using the quadrupole moment $Q = (0.220 \pm 0.015)$ barn for ^{63}Cu (Ref. 44) and the asymmetry parameter $\eta = (V_{xx} - V_{yy})/V_{zz} = 0.885$ from the FPLO calculation

$$\nu_Q = \frac{3}{2I(2I-1)} \frac{eQV_{zz}}{h} \sqrt{1 + \frac{1}{3}\eta^2}.$$

The LSDA+*U* approach can improve the description of the correlated orbital. Its occupation becomes more polarized and the absolute value of the EFG increases, as it can be seen in Fig. 11.

Values of U between 3.5 and 5.5 eV yield a good agreement of the measured V_{zz} and the calculated one. This is in agreement with band-structure calculations performed for other cuprates. There is a basically constant shift[45] in U for a series of low-dimensional Cu^{2+} systems: the value of U needed to describe the EFG correctly is about 2 eV smaller than the value of U needed to describe the (nearest-neighbor) exchange integral J correctly.[25]

The strong local distortion is not only in line with the large EFG but also with a large asymmetry parameter η, ($0 \leq \eta \leq 1$), which essentially does not change for the physically relevant range of U (inset of Fig. 11). The calculated, rather large EFG naturally raises the question about the underlying origin with respect to the crystal structure, especially the local Cu environment. Since the EFG is mostly determined by the site symmetry and the distance to the nearest-neighbor atoms, we investigated to what extent the

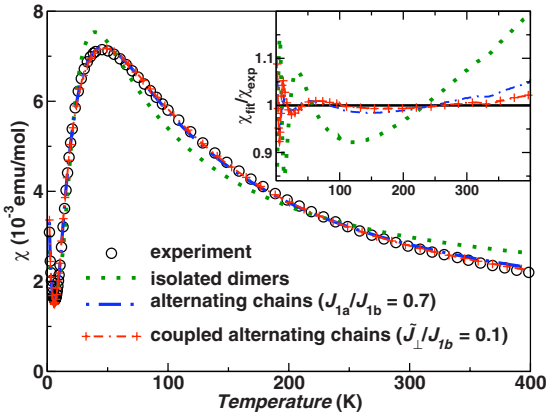

FIG. 12. (Color online) Fits (lines) to the experimental magnetic susceptibility (circles, only one of each five measured points is shown) using different models: isolated dimers, alternating Heisenberg chains, and coupled alternating Heisenberg chains. All fits include the temperature-independent term χ_0 and the impurity contribution C/T. Inset: normalized values $\chi_{\mathrm{fit}}/\chi_{\mathrm{exp}}$ (yield 1 for an ideal fit) are shown to underscore the difference between the fits.

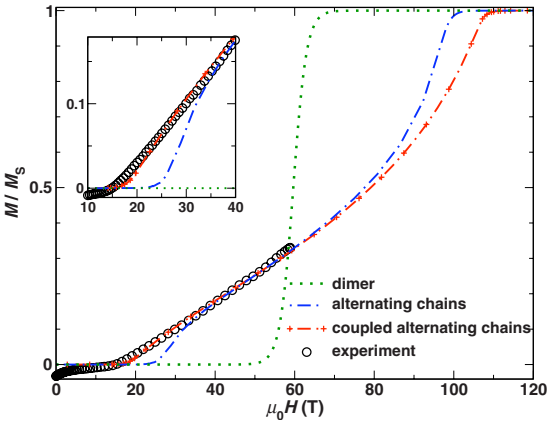

FIG. 13. (Color online) High-field magnetization curve $M(H)$ for $Cu_2(PO_3)_2CH_2$ (circles). Theoretical magnetization curves for the isolated dimer, the alternating chain and the coupled alternating chains models. The parameters were taken from the fits to the magnetic susceptibility (Fig. 12). To account for paramagnetic impurities, the theoretical curves were vertically shifted by M_S^{imp}, defined as the magnetization at 17 T.

EFG depends on the strong distortion of the plaquettes and their linking. For that purpose we calculated several fictitious structures with different local Cu environments as well as closely related structures of real Cu^{2+} systems. However, an unambiguous assignment of the size of the EFG to a single structural characteristic seems to be impossible. Our preliminary results indicate that (i) the distortion of the plaquettes, (ii) their linking (edge-shared, corner-shared, or isolated plaquettes), and (iii) the dimensionality of the network have comparable impact on the size of the EFG. A detailed study will be presented elsewhere.[46]

4. Quantum Monte Carlo simulations and high-field magnetization measurements

To complete our computational analysis, we return to the experimental temperature dependence of the magnetic susceptibility $\chi(T)$. Despite the evidence of a gapped magnetic excitation spectrum, the experimental curve $\chi(T)$ is poorly described by the isolated dimer model[47] with only one exchange parameter $J_{1b}=5.5$ meV (see Fig. 12, dotted line). In addition, the obtained fit yields $g=1.60$ corresponding to $\mu_{\mathrm{eff}}=1.38\mu_B$ per Cu^{2+} atom, considerably smaller than the expected (pure spin) contribution $1.73\mu_B$.

In order to get better agreement with the experimental susceptibility curve, we consider a coupling between the dimers, i.e., the coupling inside a structural dimer (J_{1a}), resulting in a description of the system as an alternating Heisenberg chain (AHC). For this model, the best fit to the experimental data is obtained[48] for $J_{1b}=6.7$ meV and the alternation ratio $J_{1a}/J_{1b}\sim 0.7$. Besides a considerable improvement of the fit (see Fig. 12, dash-dotted line), the resulting $g=2.01$ seems more appropriate compared to the too small g value obtained from the isolated dimer fit.

The microscopic model evidences the presence of considerable interchain couplings. Thus, we performed the simulations of magnetic behavior for a cluster of coupled AHC using QMC. As a result, the small effective interchain coupling $\tilde{J}_\perp \sim 0.1J_{1b}$ ($J_{1b}=6.86$ meV) leads to a further improvement of the fit to the magnetic susceptibility (Fig. 12, dash dotted line with "+" signs). The resulting g-factor ($g = 2.10$) has a rather typical value for cuprates, justifying the fit.

At this point, we turn to the analysis of the high-field magnetization curve, measured at 1.5 K and shown in Fig. 13. In low fields ($\mu_0 H < 17.5$ T) $Cu_2(PO_3)_2CH_2$ resides in the singlet ground state with zero magnetization. In this field region the experimental data are dominated by paramagnetic impurities. This can be seen in a linear field dependence of the magnetization followed by a gradual crossover to saturation M_S^{imp} at approximately 5 T. At the critical field $\mu_0 H=17.5$ T the spin gap closes and the magnetization increases monotonically, without any sign of saturation or plateau up to 60 T for this temperature. The experimental value of the critical field $\mu_0 H=17.5$ T and $g=2.10$ from the $\chi(T)$ fit, yield the spin gap $\Delta_{M(H)}=25$ K in perfect agreement with the NQR value $\Delta_{^{63}(1/T_1)}=24$ K.

As the saturation field exceeds the highest experimentally accessible field, the normalized magnetization M/M_S can be estimated only by using the low-field data as reference. However, the direct mapping of the 60 T curve to the low-field (SQUID) data is hampered due to a considerable hysteresis of the 60 T curve in the overlapping region up to $\mu_0 H=9$ T. This hysteresis is related to the technique of high-field measurements, and, in principle, could be suppressed by lowering the maximal magnetic field of the pulses. Unfortunately, in case of $Cu_2(PO_3)_2CH_2$ such a calibration procedure was not successful.[49] Therefore, we simulate the M/M_S behavior at 1.5 K of an isolated dimer, an AHC, and coupled AHC, using the parameters from the fits to the magnetic susceptibility, namely, the exchange integrals and g-factors, and compare the resulting theoretical curves with the experimental data (Fig. 13).

The isolated dimer model (dotted line) clearly fails to describe the experimental data. The AHC model (dash dotted

curve) provides the correct slope, but considerably overestimates the spin gap yielding a significant deviation from the experimental data in the region $\mu_0 H = 17.5-35$ T (inset of Fig. 13). On contrary, the coupled AHC model yields a good description of the experimental curve especially in vicinity of the spin gap. Note, that the deviations between 55 and 60 T are related to larger error bars in the experimental values for $M(H)$.[50]

As a check of consistency, we estimate the spin gap Δ_{AHC} using the formula for the AHC model given without any interchain couplings by $\Delta_{\mathrm{AHC}} \approx 2\delta^{3/4}J$, where $\delta=(J_{1b}-J_{1a})/(J_{1b}+J_{1a})$ and $J=(J_{1b}+J_{1a})/2$ (see Refs. 51 and 52 for details). The resulting $\Delta_{\mathrm{AHC}} \approx$ 37 K is considerably closer to the estimates from the high-field measurements ($\Delta_{M(H)}=25$ K) and the temperature dependence of the spin-lattice-relaxation rate ($\Delta_{^{63}(1/T_1)}=24$ K), than the isolated dimer value of $\Delta_{\mathrm{dimer}} \approx 64$ K. The agreement can be further improved by taking the interchain coupling into account, as can be seen in the inset of Fig. 13.

Despite the good agreement between the experimental and calculated magnetic susceptibility for the model of effectively coupled alternating Heisenberg chains, the alternation parameter J_{1a}/J_{1b} obtained from the fit (~ 0.7) is significantly larger compared to the results of the DFT calculations (~ 0.1). This discrepancy has likely two origins: (i) the minimal character of the suggested model itself with respect to one effective interchain coupling, only and (ii) the neglect of the frustrating nature of the interchain coupling to keep the model simple and treatable for the QMC techniques. Moreover, the scaling of the experimental high-field magnetization curves could be performed only within an imperfect calibration procedure, which decreases the accuracy of the obtained parameters further. Our preliminary results indicate a rather strong influence of the interchain coupling on the spin-gap size, the saturation field and the slope of the $M(H)$ curve. Therefore, a more detailed and rigorous analysis of the interchain couplings should be carried out in future studies to further improve the description.

In conclusion, the suggested minimal microscopic model of coupled alternating Heisenberg chains based on band-structure calculations and quantum Monte Carlo simulations leads to a consistent description of the macroscopic magnetic behavior.

IV. SUMMARY AND CONCLUSIONS

In the present joint theoretical and experimental investigation we have demonstrated that the spin 1/2 system $Cu_2(PO_3)_2CH_2$ can be described in good approximation as coupled alternating antiferromagnetic Heisenberg chains. Although the structural Cu_2O_6 dimers present in this compound may on first glance suggest a strong magnetic interaction within these dimers, our study can consistently assign the leading exchange to an antiferromagnetic interdimer coupling. The reliability of the suggested unexpected scenario is based on a variety of independent experimental and theoretical methods: (i) magnetic susceptibility, (ii) specific-heat, (iii) NMR, (iv) NQR, and (v) high-field magnetization measurements that are accompanied by (vi) density-functional band-structure calculations and (vii) quantum Monte Carlo simulations to provide microscopic insight into the origin of the magnetic interactions.

Although magnetic susceptibility χ and specific-heat measurements c_p clearly evidence a spin gap, a simple dimer model is not appropriate to describe the data with reasonable accuracy. In addition, the obtained parameters are incompatible with usual Cu^{2+} magnetism. Since the temperature dependence of the measured Knight shift K is in very good agreement with the χ data (above about 10 K), the deviation of the dimer fit from the experimental data cannot be assigned to impurities or a foreign phase. Thus, stimulated by the chainlike features in the crystal structure, the simple dimer model was extended by an additional coupling resulting in an alternating Heisenberg chain model. A corresponding fit using this AHC model led to a considerable improvement, resulting in a spin gap of about 30 K, slightly depending on the method of its evaluation. NQR measurements of the spin lattice relaxation time exhibit an activation-law behavior that can be described with a spin gap of about 24 K in very good agreement with the above-mentioned value. The evaluated ^{63,65}Cu quadrupole frequencies are unusually high compared with typical values for other cuprate compounds.

To challenge the suggested model and to get microscopic insight into the main magnetic interaction paths, density-functional band-structure calculations were carried out. The combination of a tight-binding model based on Wannier functions for the relevant antibonding bands with LSDA $+U$ total-energy calculations for supercells with different spin arrangements leads consistently to an AHC model. However, the DFT calculations result in sizable, frustrated couplings between the alternating chains. For the sake of simplicity of the corresponding magnetic model, these individual couplings are represented by an effective frustrating interchain exchange that is about 5 times smaller than the leading coupling along the chains. Surprisingly, this leading antiferromagnetic exchange corresponds to the coupling *between* the structural Cu_2O_6 dimers. The coupling *within* these dimers is strongly reduced due to sizable ferromagnetic contributions. Our findings underline again the impending danger to obtain an inappropriate magnetic model based on over-simplified structural considerations, i.e., regarding interatomic distances, only. The reliability of our first-principles calculations is supported by the theoretically evaluated electric field gradient which is in good agreement with the measured quadrupole frequency.

Our study is completed by quantum Monte Carlo simulations that are in line with the proposed model of coupled alternating chains. Simulating the high-field magnetization curve using QMC calculations, we demonstrated that the suggested interchain coupling leads to a considerable improvement with respect to the measured data, especially in the vicinity of the spin gap.

In conclusion, the reported study of $Cu_2(PO_3)_2CH_2$ finds a spin singlet ground state and consistently describes it by a model of coupled alternating Heisenberg chains. To get further insight into the complex interplay of structural features and the magnetic properties of this compound, single-crystal measurements and low-temperature structural investigations,

especially regarding the coalescence of the two ^{31}P NMR lines below 10 K, are highly desirable. In particular, our approach underlines that the assignment of the proper magnetic model can largely benefit from the combination of various experimental techniques with a detailed microscopic analysis based on modern band-structure theory.

ACKNOWLEDGMENTS

The authors acknowledge the financial support from Russian Science Support Foundation and Russian Ministry of Science and Education (Contract No. 01.740.11.0219, A. A. G. and K. S. O.), the Emmy-Noether-program (H. R.) and the Max-Planck Society (Project No. M.FE.A.CHPHSM, F. W.). We also thank U. Nitzsche for the use of the computational facilities at the IFW Dresden, and A. Tsirlin, F. Haarmann, R. Kniep, and A. Möller for fruitful discussion. Part of this work has been supported by EuroMagNET II under the EU contract.

[1] D. C. Johnston, J. W. Johnson, D. P. Goshorn, and A. J. Jacobson, Phys. Rev. B **35**, 219 (1987).
[2] A. W. Garrett, S. E. Nagler, D. A. Tennant, B. C. Sales, and T. Barnes, Phys. Rev. Lett. **79**, 745 (1997).
[3] R. Melzi, P. Carretta, A. Lascialfari, M. Mambrini, M. Troyer, P. Millet, and F. Mila, Phys. Rev. Lett. **85**, 1318 (2000).
[4] H. Rosner, R. R. P. Singh, W. H. Zheng, J. Oitmaa, S.-L. Drechsler, and W. E. Pickett, Phys. Rev. Lett. **88**, 186405 (2002).
[5] A. Bombardi, J. Rodriguez-Carvajal, S. DiMatteo, F. de Bergevin, L. Paolasini, P. Carretta, P. Millet, and R. Caciuffo, Phys. Rev. Lett. **93**, 027202 (2004).
[6] T. Masuda, A. Zheludev, A. Bush, M. Markina, and A. Vasiliev, Phys. Rev. Lett. **92**, 177201 (2004).
[7] A. A. Gippius, E. N. Morozova, A. S. Moskvin, A. V. Zalessky, A. A. Bush, M. Baenitz, H. Rosner, and S.-L. Drechsler, Phys. Rev. B **70**, 020406(R) (2004).
[8] S.-L. Drechsler, J. Málek, J. Richter, A. S. Moskvin, A. A. Gippius, and H. Rosner, Phys. Rev. Lett. **94**, 039705 (2005).
[9] T. Masuda, A. Zheludev, A. Bush, M. Markina, and A. Vasiliev, Phys. Rev. Lett. **94**, 039706 (2005).
[10] A. A. Tsirlin and H. Rosner, Phys. Rev. B **79**, 214416 (2009).
[11] H. Kageyama, T. Kitano, N. Oba, M. Nishi, S. Nagai, K. Hirota, L. Vicitu, J. B. Wiley, J. Yasuda, and Y. Baba, J. Phys. Soc. Jpn. **74**, 1702 (2005).
[12] H. Kageyama, J. Yasuda, T. Kitano, K. Totsuka, Y. Narumi, H. Hagiwara, K. Kindo, Y. Baba, N. Oba, and Y. Ajiro, J. Phys. Soc. Jpn. **74**, 3155 (2005).
[13] K. Barthelet, M. Nogues, D. Riou, and G. Ferey, Chem. Mater. **14**, 4910 (2002).
[14] Y. Miura, R. Hirai, Y. Kobayashi, and M. Sato, J. Phys. Soc. Jpn. **75**, 084707 (2006).
[15] H. Koo and M.-H. Whangbo, Inorg. Chem. **47**, 128 (2008).
[16] S. Derakhshan, H. L. Cuthbert, J. E. Greedan, B. Rahaman, and T. Saha-Dasgupta, Phys. Rev. B **76**, 104403 (2007).
[17] D. A. Tennant, S. E. Nagler, A. W. Garrett, T. Barnes, and C. C. Torardi, Phys. Rev. Lett. **78**, 4998 (1997).
[18] See supplementary material at http://link.aps.org/supplemental/10.1103/PhysRevB.81.104416 for the full crystallographic data.
[19] D. Eckert, R. Grössinger, M. Doerr, F. Fischer, A. Handstein, D. Hinz, H. Siegel, P. Verges, and K.-H. Müller, Physica B **294-295**, 705 (2001).
[20] K. Koepernik and H. Eschrig, Phys. Rev. B **59**, 1743 (1999).
[21] J. P. Perdew and Y. Wang, Phys. Rev. B **45**, 13244 (1992).
[22] H. Eschrig, K. Koepernik, and I. Chaplygin, J. Solid State Chem. **176**, 482 (2003).
[23] A. I. Liechtenstein, V. I. Anisimov, and J. Zaanen, Phys. Rev. B **52**, R5467 (1995).
[24] K. Koch, R. O. Kuzian, K. Koepernik, I. V. Kondakova, and H. Rosner, Phys. Rev. B **80**, 125113 (2009).
[25] K. Koch, Ph.D. thesis, University of Technology Dresden, 2009.
[26] A. F. Albuquerque, F. Alet, P. Corboz, P. Dayal, A. Feiguin, S. Fuchs, L. Gamper, E. Gull, S. Gürtler, A. Honecker, R. Igarashi, M. Körner, A. Kozhevnikov, A. Läuchli, S. R. Manmana, M. Matsumoto, I. P. McCulloch, F. Michel, R. M. Noack, G. Pawlowski, L. Pollet, T. Pruschke, U. Schollwöck, S. Todo, S. Trebst, M. Troyer, P. Werner, and S. Wessel, J. Magn. Magn. Mater. **310**, 1187 (2007).
[27] B. Bleaney and K. D. Bowers, Proc. R. Soc. London, Ser. A **214**, 451 (1952).
[28] T. Shimizu, J. Phys. Soc. Jpn. **62**, 772 (1993).
[29] T. Shimizu, J. Phys. Soc. Jpn. **62**, 779 (1993).
[30] K. Hanzawa, J. Phys. Soc. Jpn. **62**, 3302 (1993).
[31] T. Imai, E. A. Nytko, B. M. Bartlett, M. P. Shores, and D. G. Nocera, Phys. Rev. Lett. **100**, 077203 (2008).
[32] E. Ehrenfreund, E. Rybaczewski, A. Garito, and A. Heeger, Phys. Rev. B **7**, 421 (1973).
[33] S. Sachdev, Phys. Rev. B **50**, 13006 (1994).
[34] A. W. Sandvik, Phys. Rev. B **52**, R9831 (1995).
[35] K. Ishida, Y. Kitaoka, Y. Tokunaga, S. Matsumoto, K. Asayama, M. Azuma, Z. Hiroi, and M. Takano, Phys. Rev. B **53**, 2827 (1996).
[36] A. Gippius, A. Moskvin, M. Baenitz, S.-L. Drechsler, E. Morozova, and H. Otto, Europhys. Lett. **63**, 282 (2003).
[37] R. Nath, A. V. Mahajan, N. Büttgen, C. Kegler, A. Loidl, and J. Bobroff, Phys. Rev. B **71**, 174436 (2005).
[38] M. D. Johannes, J. Richter, S.-L. Drechsler, and H. Rosner, Phys. Rev. B **74**, 174435 (2006).
[39] O. Janson, R. O. Kuzian, S.-L. Drechsler, and H. Rosner, Phys. Rev. B **76**, 115119 (2007).
[40] M. Schmitt, S. Gerlach, O. Janson, M. Schmidt, W. Schnelle, J. Richter, and H. Rosner (unpublished).
[41] In the related compounds with similar bandwidths and isolated plaquettes comparable values for U_{eff} were chosen: $Sr_2Cu(PO_4)_2$ – U_{eff}=4.5 eV and Bi_2CuO_4 – U_{eff}=4–5 eV.
[42] J. Kanamori, Prog. Theor. Phys. **17**, 177 (1957).
[43] We obtained $J_\perp$ by averaging the calculated individual exchange integrals. All calculated individual contributions are of similar size between 1 and 2 meV, but have a rather large error bar ($\sim$50%) due to the small energy differences and the computationally limited size of supercells.

[44] P. Pyykkö, Mol. Phys. **99**, 1617 (2001).
[45] This shift in U is code independent. Although a local orbital and a plane-wave code need different absolute values for U to describe the EFG or the exchange J due to their different basis implementation, the shift in U for both basis schemes is basically the same.
[46] K. Koch, M. Schmitt, K. Koepernik, and H. Rosner (unpublished).
[47] For the magnetic susceptibility of an isolated dimer, we use the formula $\chi^*(t)=[t(3+e^{(t^{-1})})]^{-1}$, with $\chi^*(t)=\chi(t)J_{1b}/Ng^2\mu_B^2$ and $t=k_BT/J$ from Ref. 51.
[48] For the fit, we used the parametrized solutions for the AF-AF (Ref. 51) and the FM-AF (Ref. 53) alternating chain models.
[49] We measured additional magnetization curves with pulses up to 16 and 32 T. Although the 16 T curve could be perfectly fitted to the low-field SQUID data, the 32 T curve again showed similar discrepancies to the SQUID data as the 60 T data.
[50] The theoretical curve for the coupled AHC model provides an estimate for the saturation field of $\mu_0 H_S \approx 110$ T, which unfortunately is out of reach with the present experimental setup.
[51] D. C. Johnston, R. K. Kremer, M. Troyer, X. Wang, A. Klümper, S. L. Bud'ko, A. F. Panchula, and P. C. Canfield, Phys. Rev. B **61**, 9558 (2000).
[52] T. Barnes, J. Riera, and D. A. Tennant, Phys. Rev. B **59**, 11384 (1999).
[53] J. J. Borras-Almenar, E. Coronado, J. Curely, R. Georges, and J. C. Gianduzzo, Inorg. Chem. **33**, 5171 (1994).